Multiple scattering effects on the EXAFS of Ge nanocrystals

2008 J. Phys.: Condens. Matter 20 165210

(http://iopscience.iop.org/0953-8984/20/16/165210)

IOP Publishing Journal of Physics: Condensed Matter

J. Phys.: Condens. Matter **20** (2008) 165210 (9pp) doi:10.1088/0953-8984/20/16/165210

Multiple scattering effects on the EXAFS of Ge nanocrystals

L L Araujo[1], G J Foran[2] and M C Ridgway[1]

[1] Department of Electronic Materials Engineering, Research School of Physical Sciences and Engineering, The Australian National University, Canberra, ACT 0200, Australia
[2] Australian Nuclear Science and Technology Organisation, Menai, NSW 2234, Australia

E-mail: lla109@rsphysse.anu.edu.au

Received 31 January 2008, in final form 11 March 2008
Published 31 March 2008
Online at stacks.iop.org/JPhysCM/20/165210

Abstract

We present a detailed extended x-ray absorption fine structure (EXAFS) spectroscopy study on the influence of multiple scattering effects on the analysis of bulk polycrystalline Ge (c-Ge) and of four Ge nanocrystal (NC) distributions with mean sizes from 4 to 9 nm. A complete description of the EXAFS signal up to the third shell of nearest neighbours for both c-Ge and Ge NCs is only achieved by including at least two double scattering and one triple scattering path. Unlike reports for bulk semiconductors and Ge–Si quantum dots, our results show that including only the most prominent double scattering path is insufficient for accurately ascertaining the structural parameters of the second and third shells, leading to unphysically small coordination numbers for the NCs. The same is observed when no multiple scattering paths are taken into account. The size dependence of the interatomic distance distributions up to the third shell of nearest neighbours has been determined for the first time. A greater reduction in coordination numbers and higher structural disorder were observed for the outer shells, reflecting the increase of the surface-to-volume ratio and reinforcing the presence of an amorphous Ge layer between the SiO_2 matrix and the NCs.

(Some figures in this article are in colour only in the electronic version)

1. Introduction

The study of nanoscale systems has attracted much attention due to the unique properties they exhibit [1–3]. For example, amorphous silica (a-SiO_2) layers embedded with Ge nanocrystals (NCs), which comprise the system under study in this contribution, emit light [4] and trap charge [5], making them suitable for the development of new optoelectronic and nonvolatile memory devices. Such properties are critically dependent on the size of the NC where a difference of several nanometres may cause a significant change in the observed properties [3]. Therefore, careful size-dependent studies on the structural properties of NCs are required not only from the fundamental aspect of characterizing size and surface related effects but also for the prospect of technological integration.

Extended x-ray absorption fine structure (EXAFS) spectroscopy is a very well suited technique for the study of nanoscale systems, as previously demonstrated [6, 7]. Since EXAFS probes short range order, it is applicable to both amorphous and crystalline materials, as well as for systems containing different degrees of crystallinity. Structural information for the first nearest neighbour (NN) shell surrounding the absorbing atom is generally obtained using a single scattering (SS) approach, while information for higher NN shells can only be reliably obtained from a multiple scattering (MS) analysis [8]. Going beyond the first NN shell in a NC size-dependent study is highly desirable for the effects of the higher surface-to-volume ratio are more pronounced for the outer shells. For NCs, where the influence of under-coordination of surface atoms and surface reconstruction are expected to increase with decreasing size, the importance of MS effects would in principle be expected to decrease as the particle size decreases. Nevertheless, it has been shown for small Pt NCs (diameters from 2 to 6 nm), for example, that MS effects are not negligible and must be considered [7, 9]. A similar conclusion was suggested for Ge–Si self-assembled quantum dots (QDs) in [10], with the difference that only the most prominent MS path was considered significant. This procedure was based on the analysis of crystalline Ge (c-Ge), where it was argued that including only the most prominent

MS path yielded the same results as including that path plus six others.

For this contribution we performed EXAFS measurements for bulk c-Ge and, for the first time, for embedded Ge NCs with four different sizes (4, 5, 6 and 9 nm diameters) and analysed the data with three different approaches to verify the presence and evaluate the importance of MS effects. The case of embedded Ge NCs is particularly interesting because recent x-ray absorption near edge structure (XANES) analyses suggested that surface reconstruction in this system may happen through the formation of amorphous-like layers [11, 12]. Our results indicate that MS effects are present and must be taken into account for all cases. Considering only the most prominent MS path may lead to inaccurate results, especially in the case of Ge NCs. Further characterization of the NCs with other techniques like transmission electron microscopy (TEM), small angle x-ray scattering (SAXS), Rutherford backscattering spectrometry (RBS) and Raman spectrometry will be published elsewhere [11, 12].

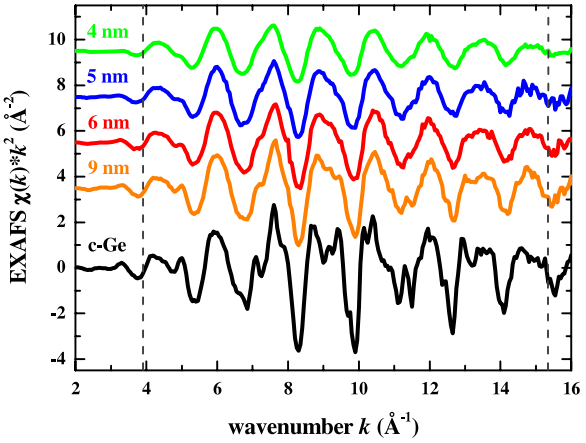

Figure 1. EXAFS oscillations (multiplied by k^2) obtained after background removal. Spectra have been vertically offset for clarity. The dashed lines indicate the k-range used for the Fourier transforms.

2. Experimental details

Amorphous SiO_2 layers of thickness 2.0 μm were grown on Si(100) substrates by wet thermal oxidation. ^{74}Ge ions were then introduced into the SiO_2 layers by ion implantation at 2.0 MeV to a total fluence of 1×10^{17} ions cm^{-2} (at liquid N_2 temperature). Afterwards, NC precipitation and growth were promoted by thermal annealing under forming gas (5% H_2 in N_2). Different combinations of annealing temperatures (between 1060 and 1100 °C) and times (between 0.33 and 10 h) were used to yield four different Ge NC distributions with sizes varying from 4.0 to 9.0 nm, as verified by SAXS measurements [11]. The Ge peak concentration was ∼3 at% at a depth of 1.4 μm beyond the SiO_2 surface, as measured by RBS [12].

After NC growth, samples for fluorescence-mode EXAFS measurements were prepared by removing the Si substrate through a combination of mechanical grinding and selective chemical etching in KOH. The thin SiO_2 layers were then stacked together between Kapton tape. This sample preparation method provides both an increased effective Ge areal density and the elimination of scattering from the Si substrate, resulting in a significant improvement in the signal-to-noise ratio and enabling high resolution measurements. A bulk polycrystalline Ge sample suited to fluorescence EXAFS was also prepared, following the method described in [13].

Fluorescence-mode EXAFS measurements at the Ge K-edge (11.103 keV) were performed at beamline 20-B of the Photon Factory, Japan. Experimental spectra were acquired at 15 K and recorded with a 6 × 6 pixel array Ge detector. The Si(111) monochromator was detuned by 50% for harmonic rejection. For energy calibration a c-Ge reference foil was concomitantly measured in transmission mode at the third ionization chamber.

3. Data analysis

The raw EXAFS spectra were first averaged and energy calibrated to the reference foil signal using the AVERAGE program [14]. Next, the EXAFS oscillations were extracted from the experimental spectra by background subtraction (removing the raw absorbance) via the AUTOBK algorithm, as implemented in ATHENA [15]. Figure 1 shows the k^2-weighted EXAFS oscillations for the c-Ge and Ge NCs samples after background removal (where k is the photoelectron wavenumber). Clearly the signal quality is very good over the measured k-range (16 Å^{-1}) even for the smallest Ge NCs. The EXAFS signal for the bulk c-Ge standard was then used to refine the values of the energy shift parameter ΔE_0 according to the procedure suggested in [16]. This enabled the alignment of the k-scale of the c-Ge theoretical standard generated by the FEFF8 code [8] for all samples and avoided errors in the structural parameters due to a poor choice of the edge energy position E_0. This was performed using ARTEMIS [15]. ATHENA and ARTEMIS are graphical user interfaces (GUIs) for the IFEFFIT code [17]. Structural parameters (mean value R, variance σ^2 and asymmetry C_3 of the distance distribution) for the first three NN shells were then determined using ARTEMIS. The Fourier transform window used for k space was of the Hanning type, with width 0.8 Å^{-1} and range 4.1–15.1 Å^{-1}. The window defining the fitting region in the non-phase-corrected radial distance R space was also of the Hanning type, with width 0.2 Å and range 1.5–4.8 Å. Effective scattering amplitudes and phase shifts were calculated *ab initio* with FEFF8 [8]. Coordination numbers were fixed to bulk values for the c-Ge analysis and fitted for the Ge NCs. Individual interatomic distances were determined for each NN shell instead of relating them all to a single lattice parameter, since experimental evidence shows that due to surface reconstruction the embedded Ge NCs are not well represented by an homogeneous lattice from surface to core [12]. Individual Debye–Waller factor and third cumulant values were also determined for each NN shell. Each given data set was fitted simultaneously with multiple k weightings of 1–4 to reduce correlations between the fitting parameters. The passive electron reduction factor S_0^2 and the energy shift parameter ΔE_0 were determined from the c-Ge data and kept

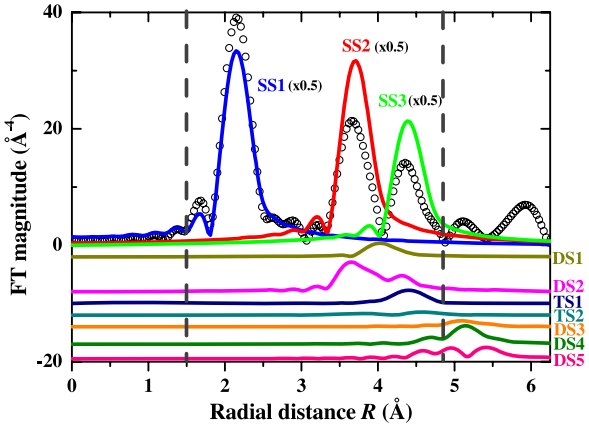

Figure 2. Fourier transformed EXAFS signal measured for c-Ge (symbols) and scattering paths calculated by FEFF8 (solid lines). SS means single scattering, DS means double scattering and TS means triple scattering. The SS paths were multiplied by 0.5 in order to make the figure clearer. The vertical dashed lines indicate the region of interest (up to the third NN shell) in this work.

constant in the Ge NCs fits. The same ΔE_0 was assigned for all paths, since charge distribution effects are not expected [18]. The values obtained were $S_0^2 = 0.99 \pm 0.05$ and $\Delta E_0 = 0.3 \pm 1.1$ eV.

Figure 2 shows the Fourier transformed (k^3-weighted) c-Ge EXAFS experimental spectrum (symbols) up to 6 Å, where the first four NN shells are visible. The vertical dashed lines indicate the region of interest for this work, up to the third NN shell. This choice was based on the fact that further NN shells were not visible in the spectra of the smaller Ge NCs. Together with the experimental spectrum, the first ten photoelectron scattering paths (full lines) as given by the FEFF8 code are also plotted in figure 2. Table 1 lists the atoms comprising each scattering path as well as the half path lengths R_{eff} and degeneracies N. The predicted relevance of each path can be observed in the figure, since it is proportional to their calculated amplitude. The single scattering paths for the first three NN shells (SS1, SS2 and SS3, respectively), superimposed to the experimental spectrum and multiplied by 0.5 in the figure, obviously comprise the dominant part of the EXAFS signal. Nevertheless, the first two double scattering (short triangular) paths, DS1 and DS2, and the first triple scattering (collinear) path TS1 have non-negligible amplitudes. As for the other paths, the second triple scattering path TS2 is still inside the region of interest but has very low amplitude while the further double scattering paths (DS3, DS4 and DS5) have somewhat higher amplitudes but lie mainly outside the fitting region (defined by the dashed lines). Note that all calculated paths shown in the figure have been given a ΔE_0 value of 0.3 eV as determined from the c-Ge sample.

In this study we performed three different fitting procedures to obtain the structural parameters for the first three NN shells. By comparing the results from each approach we will then evaluate the influence of multiple scattering in the EXAFS of c-Ge and Ge NCs, noting the latter has not been determined previously. In the first procedure, only the SS paths were taken into account, henceforth referred to as the

Table 1. Photoelectron scattering paths for the diamond lattice of c-Ge as given by the FEFF8 code. Ge^0 denotes the central absorbing atom and Ge^1, Ge^2 and Ge^3 denote first, second and third NN, respectively. Ge^{1*} denotes a first shell atom different from Ge^1 and $Ge^{1\#}$ denotes a first shell atom which is not also a first NN of Ge^2.

Notation	Path	R_{eff} (Å)	N (atoms)
SS1	Ge^0–Ge^1–Ge^0	2.4500	4
SS2	Ge^0–Ge^2–Ge^0	4.0008	12
SS3	Ge^0–Ge^3–Ge^0	4.6914	12
DS1	Ge^0–Ge^1–Ge^{1*}–Ge^0	4.4504	12
DS2	Ge^0–Ge^2–Ge^1–Ge^0	4.4504	24
TS1	Ge^0–Ge^1–Ge^0–Ge^1–Ge^0	4.9000	4
TS2	Ge^0–Ge^1–Ge^2–Ge^1–Ge^0	4.9000	12
DS3	Ge^0–Ge^2–$Ge^{1\#}$–Ge^0	5.5711	48
DS4	Ge^0–Ge^3–Ge^1–Ge^0	5.5711	48
DS5	Ge^0–Ge^3–Ge^2–Ge^0	5.5711	48

'No MS' procedure. In the second procedure, called 'Full MS', all (seven) paths that lie in the region of interest were used-SS1, SS2, SS3, DS1, DS2, TS1, TS2. In the last procedure, only the most prominent multiple scattering path, DS2, was included together with the three SS paths. This procedure, named 'Only DS2', aims to assess the validity of the claim made by Sun and Wei in [10, 19] that for bulk binary semiconductors with the zinc-blend structure, as well as for c-Ge and Ge–Si QDs, the inclusion of only the DS2 path yields the same structural parameters as if all multiple scattering paths are included.

For the multiple scattering analyses, not all parameters can be individually floated. We have restrained the MS path parameters as functions of the floating SS path parameters for the shells involved in the respective MS paths. The coordination numbers and interatomic distances were constrained to follow the geometrical conditions described in table 1, so that we have $CN_{\text{DS1}} = 3CN_{\text{TS1}} = CN_{\text{TS2}} = 3CN_{\text{SS1}}$, $CN_{\text{DS2}} = CN_{\text{SS1}}(CN_{\text{SS2}}/2)$, $R_{\text{DS1}} = R_{\text{DS2}} = (2R_{\text{SS1}} + R_{\text{SS2}})/2$ and $R_{\text{TS1}} = R_{\text{TS2}} = (4R_{\text{SS1}})/2$. Furthermore, MS paths with the same R_{eff} (DS1 and DS2-TS1 and TS2) were constrained to have the same Debye–Waller factors, written as the quadratic mean of the individual SS Debye–Waller factors, and the same third cumulant values, written as the mean of the individual SS third cumulants involved in the respective paths.

4. Results and discussion

4.1. Bulk c-Ge

The structural parameters of the first three NN shells of c-Ge are presented in table 2. Each row shows the results obtained using one of the fitting procedures. The resulting fits are shown in figure 3 together with the experimental spectrum (k^3-weighted) both in Fourier transformed R (top row—a, b, c) and in back-Fourier transformed (real part) k (bottom row—d, e, f) space. The slight mismatch between fit and experiment at ∼4.7 Å and above is assigned to the contributions leaking from paths nominally outside of the R space window (like DS4 and DS5).

As expected, the results obtained for the first NN shell are completely insensitive to the fitting procedure applied, since

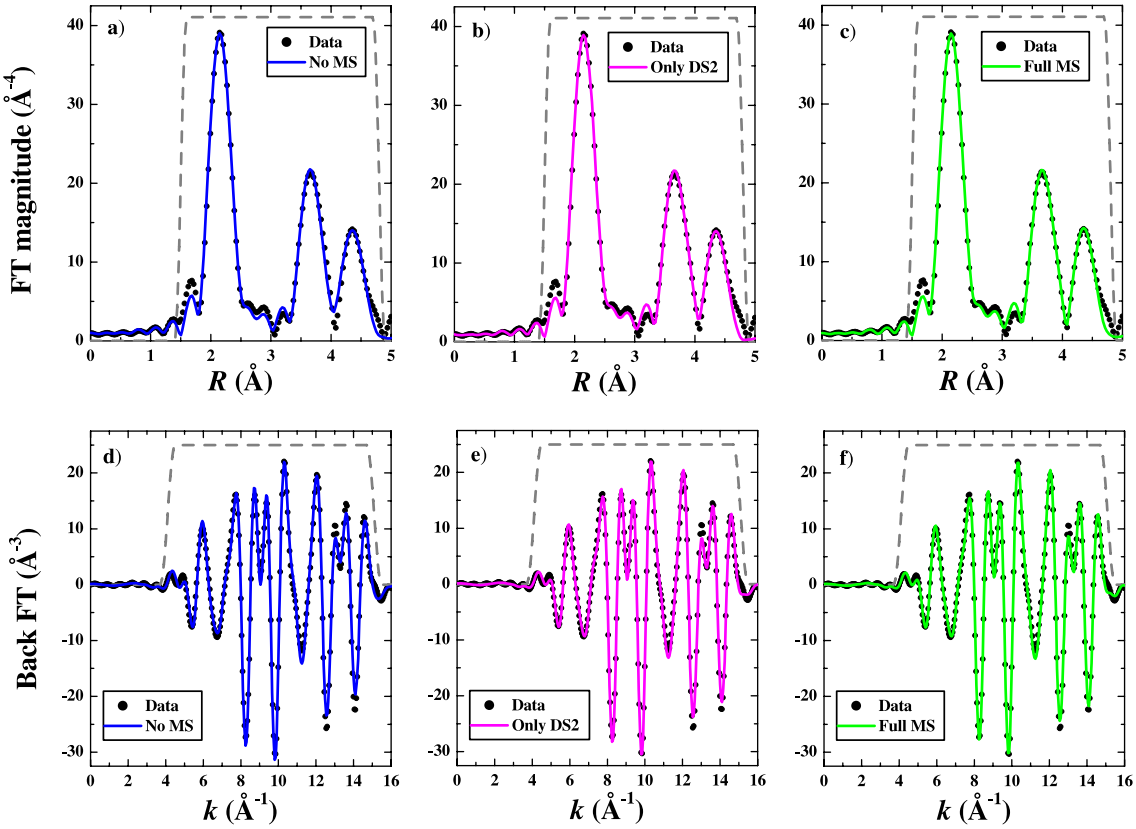

Figure 3. Fourier transformed (top row—a, b, c) and back-Fourier transformed real part (bottom row—d, e, f) EXAFS signal (k^3-weighted) for the c-Ge sample (symbols) and fits using the three procedures proposed in the text, as indicated in the legends. The dashed lines indicate the filtering/fitting windows.

Table 2. Structural parameters—interatomic distances R, Debye–Waller factors σ^2 and third cumulants C_3—obtained for the first three NN shells of c-Ge by using the three different fitting procedures. The coordination numbers were fixed to bulk values (listed in table 1). The corresponding statistical goodness-of-fit is given in table 3.

	1st NN			2nd NN			3rd NN		
Fitting procedure	R (Å)	σ^2 (10^{-3} Å^2)	C_3 (10^{-4} Å^3)	R (Å)	σ^2 (10^{-3} Å^2)	C_3 (10^{-4} Å^3)	R (Å)	σ^2 (10^{-3} Å^2)	C_3 (10^{-4} Å^3)
No MS	2.434 ± 0.005	2.2 ± 0.2	-0.7 ± 0.6	4.006 ± 0.009	4.6 ± 0.4	1.4 ± 1.3	4.682 ± 0.015	4.7 ± 0.6	-0.3 ± 1.9
Only DS2	2.435 ± 0.003	2.2 ± 0.1	-0.6 ± 0.4	3.988 ± 0.007	3.9 ± 0.2	-0.4 ± 0.8	4.681 ± 0.012	5.4 ± 0.5	-0.2 ± 1.7
Full MS	2.436 ± 0.001	2.2 ± 0.1	-0.6 ± 0.3	3.991 ± 0.006	4.0 ± 0.2	-0.1 ± 0.7	4.683 ± 0.009	4.5 ± 0.3	0.1 ± 1.2

Table 3. Statistical goodness-of-fit parameters obtained for the c-Ge fits.

Fitting procedure	R-factor	Reduced χ^2
No MS	0.015	85.4
Only DS2	0.008	45.8
Full MS	0.006	32.4

the first shell is well separated from the region where MS paths play a role. This also indicates that restraining the MS paths as functions of the floating SS paths does not introduce distortions in the results obtained for the SS parameters. There is a small decrease in the fitting errors even for the first shell when MS paths are included in the fits, as apparent from the first three columns of table 2. Furthermore, the statistical 'goodness-of-fit' parameters improve significantly when more MS paths are added, as shown in table 3. We point out that here all MS parameters are restrained as combinations of the SS parameters, so that adding MS paths does not mean adding free parameters. Furthermore, the concomitant reduction of error bars even for the first NN shell suggests a real improvement in the obtained structural parameters.

The fitting results for the outer shells, on the other hand, have a non-negligible dependence on the fitting procedure, as apparent from table 2 and figure 3 (particularly in the region between the second and third peaks, at ∼4 Å). If no MS paths are included, the fitting returns virtually the same value of the Debye–Waller factor σ^2 for the second and third NN shells. In principle, this is not physically consistent for c-Ge; the third shell σ^2 should be somewhat higher than the second shell σ^2.

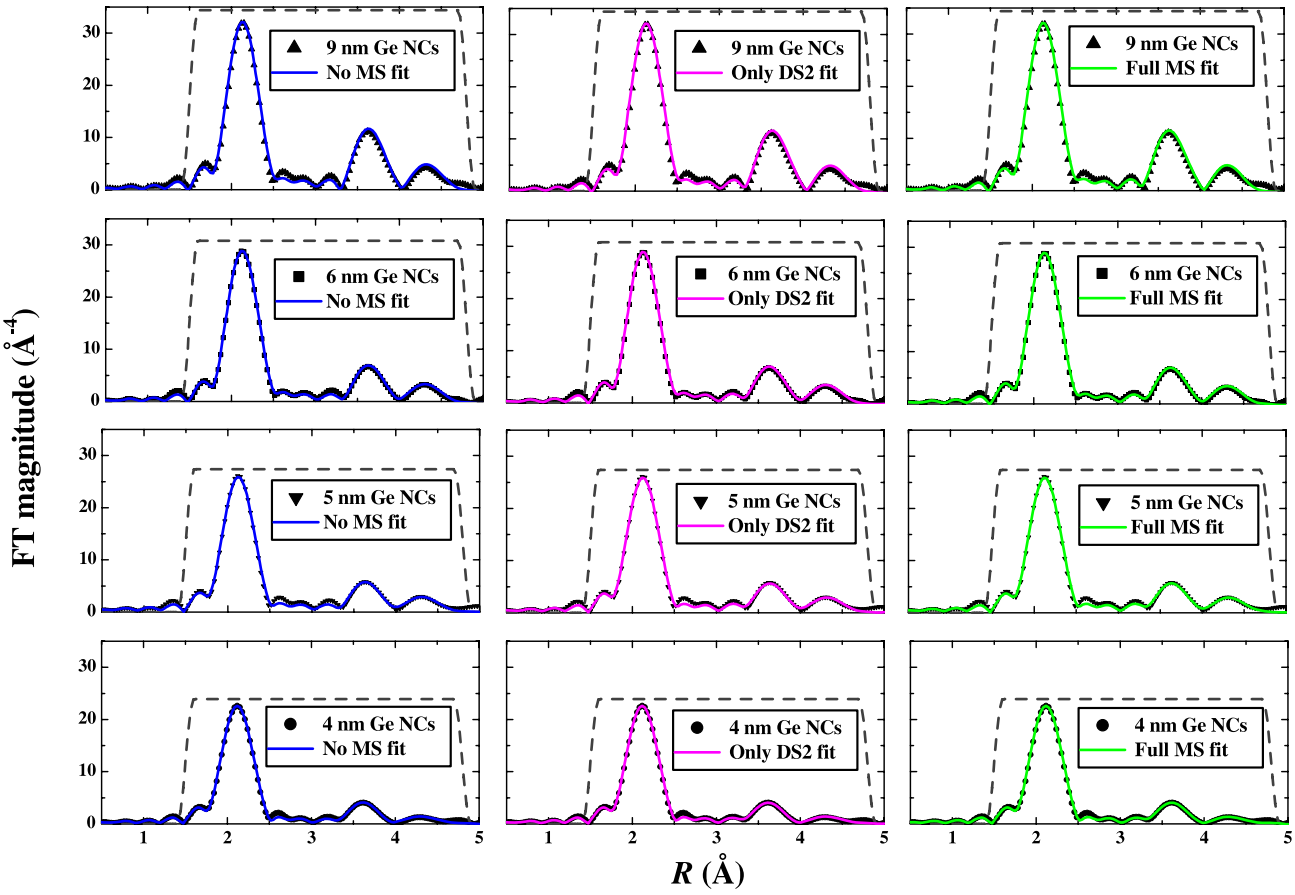

Figure 4. Fourier transformed signal (k^3-weighted) obtained form the EXAFS measurements for the Ge NCs samples (symbols) and respective fits using the three procedures proposed in the text, as indicated in the legends. The dashed lines indicate the fitting windows.

Including just the DS2 path in the fits is enough to achieve this condition; as mentioned in [10], DS2 and SS2 interfere destructively and adding DS2 to the fits remedies the higher σ^2 value obtained for the second shell when no MS paths are taken into account. But if the results of the fit including only DS2 are compared with the results of the 'Full MS' fit they are not the same, contrary to the suggestion in [10]. While for the second shell σ^2 they do yield the same value, using only DS2 actually causes a small overestimation of the value of σ^2 for the third shell, for SS3 and DS2 also overlap (figure 2). Therefore, our results for bulk c-Ge indicate that the best fits are obtained only when the 'Full MS' approach is used. Finally, we point out that if path TS2 is not included in this approach the results do not change significantly, so that it would suffice to include paths DS1, DS2 and TS1.

4.2. Ge nanocrystals

The structural parameters of the first three NN shells of the four Ge NC distributions are presented in tables 4 and 5. The corresponding fits are shown in figure 4 together with the experimental data in Fourier transformed R space (k^3-weighted). All data were plotted in the same vertical scale to clearly show the reduction in amplitude with the decrease in NC size. Despite this decrease in amplitude, both the second and third NN peaks are still visible for the smallest NCs (4 nm diameter). From the figure, it is clear that either the three fitting procedures return very similar structural values for each NC size or the visual aspect of the fits can be deceiving when higher shells and MS paths are involved. A close inspection of the values listed on tables 4–6 shows the latter assumption to be correct. If no asymmetry (no C_3) is allowed for the second and third shells, the fits for the NCs become significantly worse both visually and numerically, returning unphysical values. This happens for all fitting procedures.

As observed for c-Ge, for all Ge NC distributions the structural parameters for the first NN shell are independent of the fitting procedure, although the error bars are smaller when the Full MS approach is used (see tables 4 and 5). This leads to the same conclusions mentioned for the first shell in the preceding section.

Regarding the second and third NN shells, a clear difference is apparent between the results returned by each fitting procedure. The effect that was subtle for c-Ge becomes substantial for Ge NCs, as seen from the coordination numbers CN, for example. The inadequacy of using only the SS paths is clear due to the much reduced CN returned for the second and third shells, as shown in tables 4 and 5 and figure 5.

In figure 5 the structural parameters (symbols) obtained for all samples with the three different approaches are plotted as a function of NC characteristic size. The dashed lines represent the evolution of the coordination numbers according

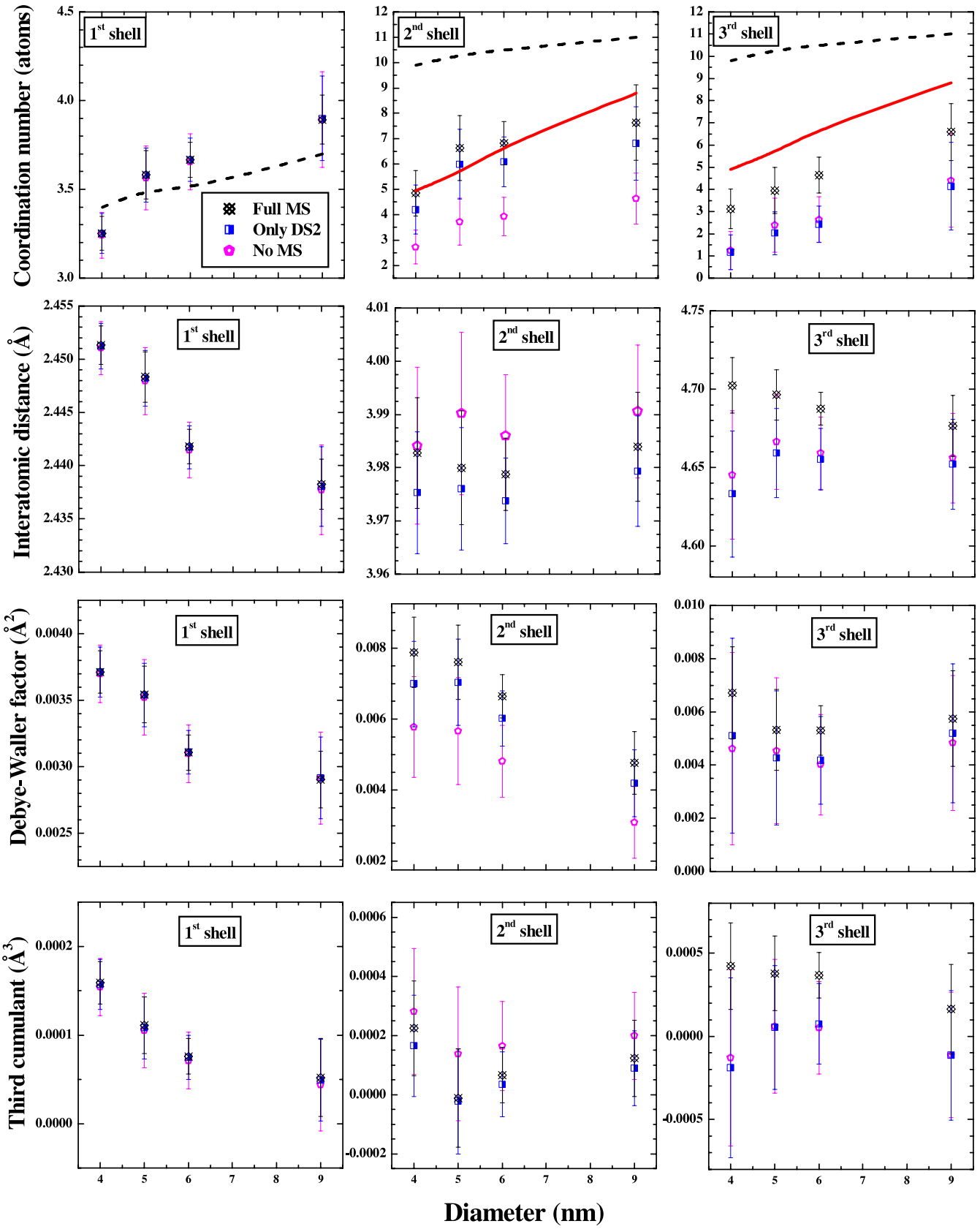

Figure 5. Structural parameters obtained for the first three NN shells of the Ge NCs (symbols) plotted as a function of NC size. Each type of symbol represents one fitting procedure, as specified in the legend. The dashed lines represent the evolution of the coordination numbers according to a geometrical model considering perfectly spherical and crystalline NCs (no surface reconstruction). The solid lines represent the same model corrected according to the fraction of crystalline atoms for each NC size as determined from XANES measurements [12].

Table 4. Structural parameters—coordination numbers CN, interatomic distances R, Debye–Waller factors σ^2 and third cumulants C_3—obtained for the first three NN shells of the Ge NCs with characteristic sizes of 9 and 6 nm with the fitting procedures specified on each column. The corresponding statistical goodness-of-fit parameters are given in table 6.

Shell		No MS	Only DS2	Full MS
		9 nm NCs		
1st NN	CN (atoms)	3.9 ± 0.3	3.9 ± 0.2	3.9 ± 0.1
	R (Å)	2.438 ± 0.004	2.438 ± 0.004	2.438 ± 0.002
	σ^2 (10^{-3} Å^2)	2.9 ± 0.4	2.9 ± 0.3	2.9 ± 0.2
	C_3 (10^{-4} Å^3)	0.4 ± 0.5	0.5 ± 0.5	0.5 ± 0.4
2nd NN	CN (atoms)	4.6 ± 1.0	6.8 ± 1.5	7.6 ± 1.5
	R (Å)	3.991 ± 0.013	3.979 ± 0.010	3.984 ± 0.009
	σ^2 (10^{-3} Å^2)	3.1 ± 1.0	4.2 ± 0.9	4.8 ± 0.9
	C_3 (10^{-4} Å^3)	2.0 ± 1.5	0.9 ± 1.3	1.2 ± 1.3
3rd NN	CN (atoms)	4.4 ± 2.1	4.1 ± 2.0	6.6 ± 1.3
	R (Å)	4.656 ± 0.029	4.652 ± 0.029	4.677 ± 0.019
	σ^2 (10^{-3} Å^2)	4.8 ± 2.5	5.2 ± 2.6	5.8 ± 1.8
	C_3 (10^{-4} Å^3)	-1.1 ± 3.8	-1.2 ± 3.8	1.6 ± 2.7
		6 nm NCs		
1st NN	CN (atoms)	3.7 ± 0.2	3.7 ± 0.1	3.7 ± 0.1
	R (Å)	2.441 ± 0.003	2.442 ± 0.002	2.442 ± 0.002
	σ^2 (10^{-3} Å^2)	3.1 ± 0.2	3.1 ± 0.2	3.1 ± 0.1
	C_3 (10^{-4} Å^3)	0.7 ± 0.3	0.8 ± 0.3	0.8 ± 0.2
2nd NN	CN (atoms)	3.9 ± 0.8	6.1 ± 1.0	6.8 ± 0.9
	R (Å)	3.986 ± 0.012	3.974 ± 0.008	3.979 ± 0.007
	σ^2 (10^{-3} Å^2)	4.8 ± 1.0	6.0 ± 0.8	6.7 ± 0.6
	C_3 (10^{-4} Å^3)	1.6 ± 1.5	0.4 ± 1.1	0.7 ± 0.9
3rd NN	CN (atoms)	2.6 ± 1.0	2.4 ± 0.8	4.6 ± 0.8
	R (Å)	4.659 ± 0.023	4.655 ± 0.020	4.688 ± 0.011
	σ^2 (10^{-3} Å^2)	4.0 ± 1.9	4.2 ± 1.6	5.3 ± 0.9
	C_3 (10^{-4} Å^3)	0.5 ± 2.8	0.8 ± 2.4	3.7 ± 1.4

to a geometrical model considering perfectly spherical and crystalline Ge NCs with the diamond structure—they do not account for surface reconstruction. The disagreement between the geometrical model and the experimental data increases dramatically for higher shells, which are most sensitive to surface effects. There is some disagreement even for the first NN shell, but this would be expected in terms of the surface reconstruction happening by the formation of an amorphous-like layer, as suggested by XANES results [12] and predicted by molecular dynamics calculations [20]. Note that for the first shell all atoms in the sample contribute to the EXAFS signal, independent of being at the crystalline core or the reconstructed surface. On the other hand, the atoms at the amorphous layer will not contribute to the signal of the second and third shells. The non-crystalline fraction of Ge atoms for each sample studied here has been estimated by a linear combination fit using bulk c-Ge and a-Ge as standards, as detailed in [12]. Such fractions were then used to correct the geometric model predictions for the second and third NN shells so that surface reconstruction/amorphization was taken into account in a first approximation. The result of this procedure is shown in figure 5 as the solid lines. It is evident from the figure that the 'No MS' fitting procedure yields CN values for the second and third NN shells that are too low compared to either the corrected or non-corrected geometric model predictions. If only the most prominent multiple scattering path (DS2) is added to the fit, the CN for the second shell improves significantly, but the CN for the third shell becomes even smaller at the same time. The best agreement is thus found only when the 'Full MS' approach is used, yielding CN for the second and third shells which are closer to predicted values.

We point out that, similarly to what is observed for c-Ge, if path TS2 is removed from the 'Full MS' fits the results do not change significantly, so that it would suffice to include paths DS1, DS2 and TS1 for Ge NCs as well.

5. Conclusions

By comparing different fitting procedures we have verified that the inclusion of MS paths is essential for a proper evaluation of the structural parameters of the first three NN shells of both c-Ge and Ge NCs. Our results further indicate that the inclusion of two double scattering (triangular) paths—DS1, DS2—and one triple scattering (collinear) path—TS1—is the best approach for the systems under study, and that including only the most prominent MS path (DS2) as suggested in [10] is insufficient and may lead to inconsistent results, in particular for the outer shells of Ge NCs. The different conclusion obtained herein relative to previous reports for c-Ge is likely due to the temperature at which the EXAFS measurements were performed. While we measured at 15 K, where thermal vibrations are minimized and a better evaluation of structural

Table 5. Structural parameters—coordination numbers CN, interatomic distances R, Debye–Waller factors σ^2 and third cumulants C_3—obtained for the first three NN shells of the Ge NCs with characteristic sizes of 5 and 4 nm with the fitting procedures specified on each column. The corresponding statistical goodness-of-fit parameters are given in table 6.

Shell		No MS	Only DS2	Full MS
		5 nm NCs		
1st NN	CN (atoms)	3.6 ± 0.2	3.6 ± 0.2	3.6 ± 0.1
	R (Å)	2.448 ± 0.003	2.448 ± 0.003	2.448 ± 0.002
	σ^2 (10^{-3} Å^2)	3.5 ± 0.3	3.5 ± 0.2	3.5 ± 0.2
	C_3 (10^{-4} Å^3)	1.0 ± 0.4	1.1 ± 0.4	1.1 ± 0.3
2nd NN	CN (atoms)	3.7 ± 0.9	6.0 ± 1.4	6.6 ± 1.3
	R (Å)	3.990 ± 0.015	3.976 ± 0.012	3.980 ± 0.011
	σ^2 (10^{-3} Å^2)	5.7 ± 1.5	7.0 ± 1.2	7.6 ± 1.1
	C_3 (10^{-4} Å^3)	1.4 ± 2.3	-0.2 ± 1.8	-0.1 ± 1.7
3rd NN	CN (atoms)	2.4 ± 1.2	2.0 ± 1.0	4.0 ± 1.0
	R (Å)	4.666 ± 0.030	4.659 ± 0.028	4.696 ± 0.016
	σ^2 (10^{-3} Å^2)	4.5 ± 2.7	4.3 ± 2.5	5.3 ± 1.5
	C_3 (10^{-4} Å^3)	0.6 ± 4.0	0.5 ± 3.7	3.8 ± 2.2
		4 nm NCs		
1st NN	CN (atoms)	3.2 ± 0.1	3.3 ± 0.1	3.3 ± 0.1
	R (Å)	2.451 ± 0.003	2.451 ± 0.002	2.451 ± 0.002
	σ^2 (10^{-3} Å^2)	3.7 ± 0.2	3.7 ± 0.2	3.7 ± 0.2
	C_3 (10^{-4} Å^3)	1.5 ± 0.3	1.6 ± 0.3	1.6 ± 0.2
2nd NN	CN (atoms)	2.7 ± 0.7	4.2 ± 1.0	4.8 ± 0.9
	R (Å)	3.984 ± 0.015	3.975 ± 0.011	3.982 ± 0.010
	σ^2 (10^{-3} Å^2)	5.8 ± 1.4	7.0 ± 1.2	7.9 ± 1.0
	C_3 (10^{-4} Å^3)	2.8 ± 2.1	1.7 ± 1.7	2.2 ± 1.6
3rd NN	CN (atoms)	1.2 ± 0.9	1.2 ± 0.8	3.1 ± 0.9
	R (Å)	4.645 ± 0.041	4.633 ± 0.040	4.702 ± 0.018
	σ^2 (10^{-3} Å^2)	4.6 ± 3.6	5.1 ± 3.7	6.7 ± 1.7
	C_3 (10^{-4} Å^3)	-1.3 ± 5.3	-1.9 ± 5.4	4.2 ± 2.6

Table 6. Statistical goodness-of-fit parameters obtained for the Ge NCs fits by using the fitting procedures proposed in this work.

Fitting procedure	9 nm NCs		6 nm NCs		5 nm NCs		4 nm NCs	
	R-factor	Reduced χ^2	R-factor	Reduced χ^2	R-factor	Reduced χ^2	R-factor	Reduced χ^2
No MS	0.009	107.3	0.004	30.9	0.006	35.5	0.004	35.6
Only DS2	0.008	85.5	0.002	18.4	0.005	25.1	0.003	26.3
Full MS	0.008	77.8	0.002	12.0	0.004	20.1	0.002	19.0

parameters is thus possible, in [10] the EXAFS measurements were performed at room temperature, where the amplitude of thermal vibrations is significantly higher and thus so is the variance of the distance distributions.

The fitting results indicate that the first NN shell distances can be determined with a precision better than 0.004 Å for both c-Ge and Ge NCs. This reflects the good quality of the experimental data and the adequacy of using the FEFF8/IFEFFIT theoretical standard and fitting procedures for c-Ge and Ge NCs. For the outer shells this factor is gradually reduced, being ten times worse for the third shell of the 4 nm NCs. In a similar way, increases in the uncertainty of the coordination numbers, Debye–Waller factors and third cumulants are also verified for the outer shells, as expected. Nevertheless, definite trends with size have been identified for the Ge NCs data (figure 5), which illustrate the higher impact on the second and third shells caused by the increase of the surface-to-volume ratio and reinforce the presence of an amorphous Ge layer separating the SiO_2 matrix and the crystalline Ge NC core. The physical origin of such trends will be discussed in greater detail elsewhere [12]. For this report, we have sought to present for the first time a size-dependent, multiple-shell characterization of embedded Ge NCs and demonstrate that a full multiple scattering approach is necessary to achieve the most accurate determination of structural parameters.

Acknowledgments

The authors acknowledge the Australian Research Council and the Australian Synchrotron Research Programme for financial support. LLA acknowledges the Brazilian Research Agency CNPq for support during his academic formation.

References

[1] Michalet X, Pinaud F F, Bentolila L A, Tsay J M, Doose S, Li J J, Sundaresan G, Wu A M, Gambhir S S and Weiss S 2005 *Science* **307** 538–44
[2] Linnros J 2005 *Nat. Mater.* **4** 117–9
[3] Roduner E 2006 *Chem. Soc. Rev.* **35** 583–92
[4] Singha A, Roy A, Kabiraj D and Kanjilal D 2006 *Semicond. Sci. Technol.* **21** 1691–8
[5] Park C J, Cho K H, Yang W C, Cho H Y, Choi S H, Elliman R G, Han J H and Kim C 2006 *Appl. Phys. Lett.* **88** 071916
[6] Modrow H 2004 *Appl. Spectrosc. Rev.* **39** 183–290
[7] Frenkel A I 1999 *J. Synchrotron Radiat.* **6** 293–5
[8] Rehr J J and Albers R C 2000 *Rev. Mod. Phys.* **72** 621–54
[9] Frenkel A I, Hills C W and Nuzzo R G 2001 *J. Phys. Chem.* B **105** 12689–703
[10] Sun Z H, Wei S Q, Kolobov A V, Oyanagi H and Brunner K 2005 *Phys. Rev.* B **71** 245334
[11] Araujo L L, Giulian R, Johannessen B, Kluth P, Cookson D J, Foran G J and Ridgway M C 2007 *Adv. Synchrotron Radiat.* (July) submitted
[12] Araujo L L, Giulian R, Kluth P, Cookson D J, Foran G J and Ridgway M C 2008 *Phys. Rev.* B (January) submitted
[13] Ridgway M C, Azevedo G D, Elliman R G, Glover C J, Llewellyn D J, Miller R, Wesch W, Foran G J, Hansen J and Larsen A N 2005 *Phys. Rev.* B **71** 094107
[14] Hester J 2007 Available at http://anbf2.kek.jp/xafs-downloads.html
[15] Ravel B and Newville M 2005 *J. Synchrotron Radiat.* **12** 537–41
[16] Kelly S D and Ravel B 2007 *AIP Conf. Proc.* **882** 132–4
[17] Newville M 2001 *J. Synchrotron Radiat.* **8** 322–4
[18] Haskel D, Ravel B, Newville M and Stern E A 1995 *Physica* B **208–9** 151–3
[19] Wei S Q and Sun Z H 2005 *J. Phys.: Condens. Matter* **17** 8017–28
[20] Pizzagalli L and Galli G 2002 *Mater. Sci. Eng.* B **96** 86–9